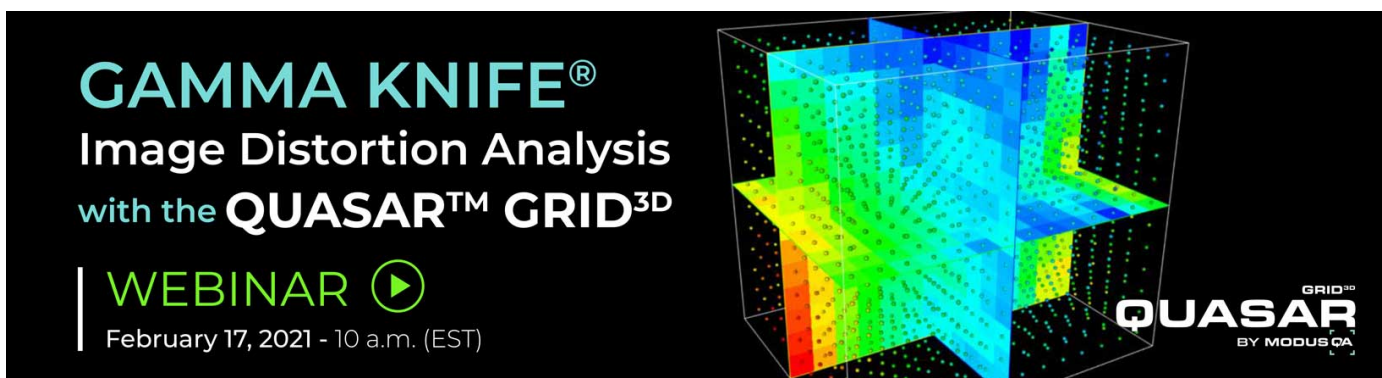


PAPER


In silico dosimetry of low-dose rate brachytherapy using radioactive nanoparticles

To cite this article: Baljeet Seniwai *et al* 2021 *Phys. Med. Biol.* **66** 045016

View the [article online](#) for updates and enhancements.



GAMMA KNIFE®
Image Distortion Analysis
with the **QUASAR™ GRID^{3D}**



WEBINAR 
February 17, 2021 - 10 a.m. (EST)

QUASAR
GRID^{3D}
BY MODUSCA



PAPER

In silico dosimetry of low-dose rate brachytherapy using radioactive nanoparticles

RECEIVED
31 August 2020REVISED
14 December 2020ACCEPTED FOR PUBLICATION
23 December 2020PUBLISHED
8 February 2021Baljeet Seniwal^{1,*} , Lucas F Freitas², Bruno M Mendes³, Ademar B Lugão², Kattesh V Katti⁴ and Telma C F Fonseca¹ ¹ Departamento de Engenharia Nuclear—Universidade Federal de Minas Gerais, Av. Antônio Carlos, 6627, Pampulha, 31270-901, Belo Horizonte, MG, Brasil² Nuclear and Energy Research Institute-IPEN/CNEN/SP, São Paulo, Brazil³ Nuclear Technology Development Center-CDTN/, BH / MG, Brasil⁴ Department of Radiology, Physics, Institute of Green Nanotechnology, University of Missouri, One Hospital Drive, Columbia, MO 65212, United States of America

* Author to whom any correspondence should be addressed.

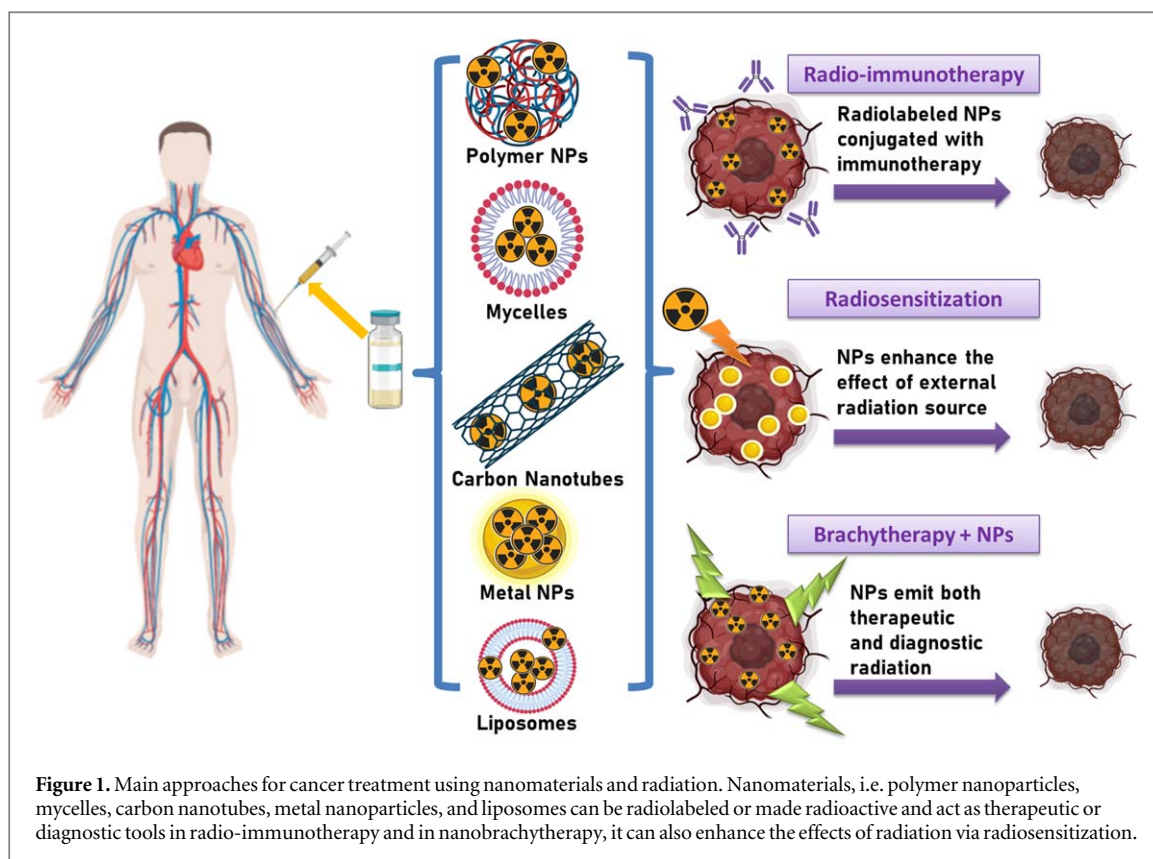
E-mail: bseniwal@eng-nucl.dout.ufmg.br and telmafonseca@nuclear.ufmg.br**Keywords:** radioactive nanoparticles, low-dose-rate brachytherapy, dosimetric calculation, single-cell dosimetry, radio-therapeutic efficiency, EGSnrc

Abstract

Purpose. Nanoparticles (NPs) with radioactive atoms incorporated within the structure of the NP or bound to its surface, functionalized with biomolecules are reported as an alternative to low-dose-rate seed-based brachytherapy. In this study, authors report a mathematical dosimetric study on low-dose rate brachytherapy using radioactive NPs. **Method.** Single-cell dosimetry was performed by calculating cellular *S*-values for spherical cell model using Au-198, Pd-103 and Sm-153 NPs. The cell survival and tumor volume versus time curves were calculated and compared to the experimental studies on radiotherapeutic efficiency of radioactive NPs published in the literature. Finally, the radiotherapeutic efficiency of Au-198, Pd-103 and Sm-153 NPs was tested for variable: administered radioactivity, tumor volume and tumor cell type. **Result.** At the cellular level Sm-153 presented the highest *S*-value, followed by Pd-103 and Au-198. The calculated cell survival and tumor volume curves match very well with the published experimental results. It was found that Au-198 and Sm-153 can effectively treat highly aggressive, large tumor volumes with low radioactivity. **Conclusion.** The accurate knowledge of uptake rate, washout rate of NPs, radio-sensitivity and tumor repopulation rate is important for the calculation of cell survival curves. Self-absorption of emitted radiation and dose enhancement due to AuNPs must be considered in the calculations. Selection of radionuclide for radioactive NP must consider size of tumor, repopulation rate and radiosensitivity of tumor cells. Au-198 NPs functionalized with Mangiferin are a suitable choice for treating large, radioresistant and rapidly growing tumors.

1. Introduction

Nanoparticles (NPs) are used in radiation therapy (RT) to enhance the radiation response or as a therapeutic or theranostic agent (Song *et al* 2017, Aranda-Lara *et al* 2020). In this regard, NPs made of high-*Z* material, especially gold nanoparticles (AuNPs), can attenuate the ionizing radiations and enhance radiation dose within the tumor. The technique of radiation dose enhancement using AuNPs is called radiosensitization (Li *et al* 2020, Schuemann *et al* 2020). Recently the enhancement in radiation dose by AuNPs is observed in brachytherapy (BT) (Ngwa *et al* 2012, 2013, Sinha *et al* 2015, Martinov *et al* 2017). It is due to the interaction of x-rays from the BT source with atoms of AuNP through the mechanism of photoabsorption. After photoabsorption the Au atoms de-excite to produce a number of emission products: photo-electrons, Auger electrons, or characteristic x-rays (Song *et al* 2017, Laprise-Pelletier *et al* 2018a).



For solid tumors such as prostate cancer, localized within the organ, seed based BT is a preferred treatment modality (Meyer *et al* 2020). Radioactive seeds of I-125/Pd-103 are permanently implanted within the prostate gland and low doses of radiation are delivered to the tumor volume for several months (Katti *et al* 2018). Seed based BT can be conjugated with AuNPs to deliver higher doses of radiation to the tumor volume. But low-dose rate BT has some limitations such as: limited options for radiation dose modulation, artifacts in radiographic images caused by metallic seeds, etc.

Recently, radioactive NPs are investigated as an alternative to low-dose rate seed based BT (Katti *et al* 2018, Aranda-Lara *et al* 2020). There are two main categories of radioactive NPs: (a) radioactive nanoparticles: the radioactive atoms are incorporated within the structure of NP, (b) radiolabeled NPs: radioactive atoms are bound to the surface of NPs (Laprise-Pelletier *et al* 2018a). Nowadays a wide range of radioactive or radiolabeled NPs are available: metallic, polymeric, lipidic, etc (presented briefly in figure 1). These NPs are either made radioactive via neutron activation technique (Katti *et al* 2018, Wang *et al* 2020) or are radiolabeled with the help of biomolecules or chelators (Aranda-Lara *et al* 2020, Su *et al* 2020) or by heat induced radiolabeling technique (Gholami *et al* 2020).

Several experimental studies have been performed to investigate the therapeutic efficiency of both radioactive and radiolabeled NPs. Authors (Chanda *et al* 2010), investigated the therapeutic efficacy of Gum arabic glycoprotein (GA) functionalized radioactive Au-198 NPs. The single dose of 70Gy was administered with intratumor injection to mice bearing human prostate xenografts. Shukla *et al* (2012), used epigallocatechin-gallate (EGCg) conjugated Au-198 NPs and performed pharmacokinetic studies in PC-3 xenograft tumors in mice. Investigators (Moeendarbari *et al* 2016), used nanoseed with core of Pd-103 coated with gold. Here also, the radiotherapeutic efficiency was tested on xenograft model of prostate cancer. Authors (L-Pelletier *et al* 2017), used two different types of radioactive NPs: (a) radioactive core of Pd-103 coated with gold, and (b) radioactive core of Pd-103 coated with radioactive Au-198 to test the therapeutic efficacy on xenograft model of prostate cancer. The NPs were functionalized with polyethylene glycol (PEG). Al-Yasiri *et al* (2017) and Katti *et al* (2018), also investigated the therapeutic efficiency on xenograft model of prostate cancer using Au-198 NPs functionalized with mangiferin (MGF). Investigators (Wang *et al* 2020), used radioactive carbon nanocapsules of Sm-153 functionalized with Cetuximab (antibody) and performed pharmacokinetic studies on melanoma lung metastatic tumor model in mice. Authors (Su *et al* 2020), utilized AuNPs radiolabeled with I-131 and twin arginine translocation (TAT) peptide to target the nuclei of the cancer cells.

The linear quadratic (LQ) model is extensively used in radiation biology to analyze and predict the response of *in vitro* and *in vivo* experiments involving ionizing radiation (McMahon 2018). The cell survival probability (S),

according to LQ formalism, following radiation exposure is described as: $S = \exp(-[\alpha D + G\beta D^2])$. Where, α and β represent the radiosensitivity of the cell, D is the radiation dose to which cell is exposed and G represents generalized Lea–Catcheside time factor (Lea and Catcheside 1942). The G -factor narrates the effects of protraction in the dose delivery in terms of DNA double strand break (DSB) repair. It can hold values from 0 to 1. Where $G = 1$ represents a single fraction of radiation dose, leading to the most common expression of the LQ model: $S = \exp(-[\alpha D + \beta D^2])$. Whereas, $G < 1$ represents the increase in S due to the repair of DSBs during the protracted treatments, similar to radiotherapy using radioactive NPs (Brenner 2008).

In case of radioactive NPs (radio-NPs) based radiotherapy (RT), the key radiobiological features are decreasing dose rate, repair of sub-lethal damage, proliferation of tumor cells and uptake and washout of radioactivity. Hence, an extended mathematical model is required to accurately estimate the probability of cell survival. Dale (1985), extended the LQ model for exponentially decreasing dose rate by including the repair rate of sub-lethal damage. Authors assumed mono-exponential rate of repair independent of irradiation time, dose and dose rate. A detailed review on the radiobiology of targeted radiotherapy (TRT) was reported by Wheldon and O’Donoghue (1990). Authors suggested that for low dose rate treatments, such as radio-NPs based RT, an approximately complete repair of sub-lethal damage can be assumed and the cell survival probability, in absence of proliferation, can be considered as an exponentially decreasing function of the dose: $S = \exp(-[\alpha D])$. It is because the repair rates of cells are generally much shorter than in comparison to the irradiation time.

Wheldon *et al* (1991), estimated the curability of tumors of different sizes using a mathematical model. It was suggested that micro-metastases may be resistant to long range beta emitters and can be effectively treated using short range emitters. O’Donoghue (1994), presented a simple mathematical model to investigate the effect of repopulation of tumor cells, on S , irradiated using mono-exponentially decreasing dose rate. This model assumed instantaneous uptake of radiopharmaceutical by tumor cells. Dale and Alejandro (2005), used the LQ model to compare the conventional radiotherapy (Fonseca *et al* 2020, Seniwal *et al* 2020) and targeted RT (Seniwal *et al* 2020a, 2020b) in terms of prescribed dose and relative biological effectiveness. Šefl *et al* (2016), extended mathematical model proposed by O’Donoghue (1994), by assuming the mono-exponential uptake and washout rate of radiopharmaceutical and investigated its effect on the cell survival. Present study makes use of the mathematical model proposed by Šefl *et al* (2016) to estimate the cell survival and tumor volume curves.

In this study we performed dosimetric calculations to determine (a) Cellular S -values (single cell dosimetry) for spherical cell model using Au-198, Pd-103 and Sm-153 NPs compared with MIRDcell database (Vaziri *et al* 2014); (b) The cell survival and tumor volume curves compared with experimental studies; (c) The radio-therapeutic efficiency of Au-198, Pd-103 and Sm-153 NPs for (i) administered radioactivity, (ii) tumor volume and (iii) tumor cell type (variable radiosensitivity and repopulation rate), as shown in table 1.

2. Methods

2.1. Cellular S -values

The cellular S -values were calculated for spherical cell geometry using EGSnrc (Kawrakow 2000) MC code following previously published methods (Seniwal *et al* 2020a) (and briefly described in table 1) for 3 radionuclides: Pd-103, Sm-153 and Au-198. The selection of radionuclides was based on the availability of experimental data on the use of radioactive nanoparticles (L-Pelletier *et al* 2017, Katti *et al* 2018, Wang *et al* 2020). The cell geometry was constructed using two concentric spheres, representing commonly used cell geometry used for single cell dosimetry. The inner sphere with radius $4 \mu\text{m}$ was considered as nucleus and outer sphere with radius $5 \mu\text{m}$ as cell. The cell geometry was placed inside another sphere of radius 1.2 times radius of the cell. All spheres were composed of unit density water. Based on the definition of S -value, point, isotropic, radioactive sources were sampled uniformly and randomly within the source region. The Evaluated Nuclear Structure Data Files (ENSDF) for the radionuclides was extracted from the national nuclear data center database (NNDC 2020). These files contained the complete decay spectrum of the radionuclides (Pd-103, Sm-153 and Au-198). These ENSDF were used to simulate the decay of radioisotopes with the help of *egs_radionuclide_source* library of EGSnrc. The calculation was performed for 5 source target combinations: (C \leftarrow C), (C \leftarrow CS), (N \leftarrow N), (N \leftarrow CY) and (N \leftarrow CS) (table 1), where C = Cell, N = Nucleus, CY = Cytoplasm and CS = Cell Surface. All calculated S -values were compared with MIRDcell database (Vaziri *et al* 2014) (presented in table 2).

2.2. Calculation of surviving fraction

For low dose rate RT techniques, such as targeted RT, the complete repair of sub-lethal damage can be expected. The cell survival curve, in the absence of proliferation, can be approximated by exponentially decreasing function of total dose D at time t ($SF(t) = \exp(-\alpha \cdot D(t))$, where $\alpha > 0[\text{Gy}^{-1}]$) (O’Donoghue 1994). Assuming that all tumor cells grow exponentially with a growth rate λ during the course of radiation treatment, and that NP uptake and washout occurs at mono-exponential rate (Dale *et al* 2007, Šefl *et al* 2016), the

Table 1. Summary of calculations performed in this study.

	Cellular S-values	Calculations for surviving fraction or tumor volume	Comparison of radiotherapeutic efficiency of Pd-103, Sm-153 and Au-198 NPs
Parameters calculated	Cellular S-values for 5 different source target combinations: cell to cell (C ← C), cell-surface to cell (C ← CS), nucleus to nucleus (N ← N), cytoplasm to nucleus (N ← CY) and cell-surface to nucleus (N ← CS).	(i) Relative tumor volume, or (ii) Tumor volume function of time based on results reported in the reference study	Relative tumor volume function of time by varying (i) Case 1: administered activities. (ii) Case 2: tumor volume (iii) Case 3: tumor cell type
Geometry Configurations	Spherical cell geometry (Seniwal et al 2020a) (i) Nucleus radius 4.0 μm (ii) cell radius 5.0 μm	Spherical tumor volume (i) L-Pelletier et al (2017): 0.27 c.c.(ii) Wang et al (2020): 0.05 c.c. (iii) Katti et al (2018): 0.03 c.c.	Spherical tumor of volume (i) Case 1: 0.3 c.c. (ii) Case 2: 0.3, 0.6 and 1.0 c.c. (iii) Case 3: 0.3 c.c.
Radionuclides considered	Pd-103, Sm-153, Au-198	Pd-103, Sm-153, Au-198	Pd-103, Sm-153, Au-198
Reference data from previous publications	Cellular S-values from (Vaziri et al 2014)	Experimental data (i) Pd-103 NPs: (L-Pelletier et al 2017) (ii) Sm-153 NPs: (Wang et al 2020) (iii) Au-198 NPs: (Katti et al 2018)	
Tumor cell lines and radio-sensitivity parameter (α)		(i) for Pd-103 NPs PC-3 cells: 0.059, 0.089, 0.107 Gy ⁻¹ (ii) for Sm-153 NPs B16F10 cells: 0.0068, 0.0102, 0.0122 Gy ⁻¹ (iii) for Au-198 NPs PC-3 cells: 0.059, 0.089, 0.107 Gy ⁻¹	(i) Case 1 and 2: PC-3 cells: 0.059 Gy ⁻¹ (ii) Case 3: PC-3 (0.059 Gy ⁻¹) and B16F10 (0.0068 Gy ⁻¹)
Activity administered		(i) L-Pelletier et al (2017): 62.9 MBq (ii) Wang et al (2020): 15.0 MBq (iii) Katti et al (2018): 0.15 MBq	(i) Case 1: 20, 40, 60 MBq (ii) Case 2 and 3: Activity was selected such that all radionuclides deposit equal absorbed dose, for Pd-103 is was fixed to 60 and 600 MBq.
Outcome	Table 2	Table 3, figure 2	Case 1: figure 3 (A)–(C); Case 2: figure 4 (A); and Case 3: figure 4 (B)

equation for cell survival curve can be written as follows:

$$SF(t) = \exp \left\{ -\alpha D_0 \left(\frac{m - k}{m \cdot k} + \frac{1}{m} \exp(-m(t - t_i)) - \frac{1}{k} \exp(-k(t - t_i)) \right) + \lambda(t - t_0) \right\}, \tag{1}$$

where: (i) $D_0(>0)$ = the extrapolated dose rate at $t = 0$, (ii) m = effective uptake rate, (iii) k = effective washout rate, (iv) t_0 = time of measuring tumor volume before intratumoral injection of radioactive NPs, (v) t_i = time of injection and (vi) α = radiosensitivity parameter. The uptake and washout rates (m and k respectively) can be estimated from the pharmacokinetic data of NPs by fitting using:

$$\%ID(t) = \%ID(\exp(-kt) - \exp(-mt)), \tag{2}$$

where %ID is the percentage of injected dose in the tumor.

The tumor growth rate (λ) can be estimated by least square fit of tumor size data of saline treated control group by:

$$N(t) = \text{const} \cdot \exp(\lambda t). \tag{3}$$

The D_0 is equal to:

$$D_0 = A \cdot ID_0 \cdot f_t \cdot S, \tag{4}$$

where A is administered radioactivity (Bq), ID_0 is fraction of mean injected dose retained in tumor volume, f_t is mass fraction (mass of tumor/(mass of organ containing tumor + mass of tumor)) and S is S-value (GyBq⁻¹.s⁻¹).

Table 2. Comparison of the cellular S -values ($\text{Gy Bq}^{-1} \cdot \text{s}^{-1}$) obtained with EGSnrc for Au-198, I-131, Pd-103, Sm-153 radionuclides with respect to MIRDcell (Vaziri *et al* 2014). Five different source-target combinations were considered: (C \leftarrow C), (C \leftarrow CS), (N \leftarrow N), (N \leftarrow CY) and (N \leftarrow CS) (table 1).

Radionuclide		S(C \leftarrow C)	S(C \leftarrow CS)	S(N \leftarrow N)	S(N \leftarrow CY)	S(N \leftarrow CS)
Pd-103	EGSnrc	1.39E-03 (-13.17%)	7.71E-04 (-13.22%)	2.42E-03 (-8.04%)	3.58E-04 (-14.38%)	2.47E-04 (-15.42%)
	MIRD-Cell	1.23E-03	6.81E-04	2.24E-03	3.13E-04	2.14E-04
Sm-153	EGSnrc	2.63E-03 (-2.33%)	1.34E-03 (12.99%)	4.52E-03 (0.22%)	1.16E-03 (-2.65%)	8.12E-04 (-14.04%)
	MIRD-Cell	2.57E-03	1.54E-03	4.53E-03	1.13E-03	7.12E-04
Au-198	EGSnrc	4.70E-04 (3.89%)	2.72E-04 (12.67%)	7.64E-04 (6.60%)	2.96E-04 (2.31%)	2.10E-04 (2.78%)
	MIRD-Cell	4.89E-04	3.11E-04	8.18E-04	3.03E-04	2.16E-04

Note. The values in round brackets represent the percentage deviation in calculated cellular S -values using EGSnrc with respect to MIRD-cell.

From the calculated surviving fraction, the tumor volume at time t ($V(t)$) can be estimated using the relation

$$V(t) = V(t_0) \cdot \text{SF}(t), \quad (5)$$

where $V(t_0)$ is measured tumor volume before injection and $\text{SF}(t)$ is surviving fraction of tumor cells at any time t . All the variables mentioned in equations (2)–(4) were calculated using the experimental data given in L-Pelletier *et al* (2017), Katti *et al* (2018), Wang *et al* (2020). Here, we calculated the α using survival fractions and α/β ratios reported in literature. Since, the α/β ratio for different tissues falls in a range, we got 3 values of α for both tumor types. Based on the findings of Wang *et al* (2020) $\alpha = 0.0068, 0.0102, \text{ and } 0.0122 \text{ Gy}^{-1}$ were used for B16F10 melanotic melanoma cells. For PC-3, prostate cancer, cells the surviving fraction after 2Gy of gamma radiation is 0.7 (Elgqvist *et al* 2016) and α/β ratio is variable between 1 and 3 (Leeuwen *et al* 2018). Based on this information α for PC-3 cells was calculated using the equation $\text{SF} = \exp(-\alpha D - \beta D^2)$. Lastly, the S -value for tumors is calculated using EGSnrc MC code, considering tumors as spherical volumes composed of water. The calculated values of all the variables are presented in table 3 and cell survival curves (or $V(t)$) are presented in figure 2.

Also, the minimum surviving fraction, SF_{\min} , is generally used to estimate the efficacy of the treatment. The time at which $\text{SF}(t) = \text{SF}_{\min}$ is defined as the critical time (t_c). It is the time in which the derivative of $\text{SF}(t)$ with respect to time goes to zero:

$$\frac{d}{dt} \text{SF}(t) = \text{SF}(t) [\lambda - \alpha D_0 (\exp(-k(t - t_i)) - \exp(-m(t - t_i)))] = 0. \quad (6)$$

For $t < t_c$, the tumor cell sterilization dominates over proliferation of tumor cells. Whereas, for $t > t_c$, cell proliferation dominates over the cell killing. In targeted treatments using radioactive nanoparticles, the dose rate is effected by the physical decay of radionuclides and uptake and washout rates of NPs. Initially the dose rate increases with increase in the uptake and reaches to its maximum value. After that it starts decreasing due to the washout of radioactive NPs and physical decay. The dose rate at which the rate of tumor cell killing and proliferation is balanced is termed as critical dose rate, $D(t_c)$. It can be estimated by re-writing equation (6), at $t = t_c$, as:

$$D(t_c) = D_0 (\exp(-k(t_c - t_i)) - \exp(-m(t_c - t_i))) = \frac{\lambda}{\alpha}. \quad (7)$$

The equation (7) can be solved numerically to estimate t_c . The t_c , $D(t_c)$ and SF_{\min} were estimated for all cases considered in this study (see table 3 and table 5).

2.3. Radio-therapeutic efficiency of Pd-103, Sm-153 and Au-198 NPs

To compare the therapeutic efficiency of radioactive NPs three cases were considered:

- (i) Case 1: Variable administered activity: Here 0.3 c.c. tumor volume was assumed to be treated with variable radioactivity of 20 MBq, 40 MBq and 60 MBq. λ and α of PC-3 cells (table 1), and k, m calculated from Katti *et al* (2018) (table 3) were used. In this work, mangiferin (MGF) was utilized as NP tumor-targeting agent. The cell survival curves for Pd-103, Sm-153 and Au-198 were calculated using equation (1). The results are presented in figures 3(A)–(C).
- (ii) Case 2: Variable tumor volume: The activity of the radionuclides was selected such that they deposit similar absorbed dose. The activity of Pd-103 was fixed to 60 MBq (equivalent to the activity of Pd-103 brachytherapy seed). Whereas, the activity required for Au-198 and Sm-153 was estimated by using the

Table 3. Effective NP washout rate (k (d^{-1})), uptake rate (m (d^{-1})), tumor growth rate (λ (d^{-1})), S -value ($Gy\ Bq^{-1}\cdot d^{-1}$), ID_0 were calculated using the method explained in section 2 and table 1. Also, critical time (t_c (d)), critical dose rate ($D(t_c)$ ($Gy\ h^{-1}$)) and minimum survival fraction ($SE_{min}(t_c)$) were calculated considering $\alpha = 0.059\ Gy^{-1}$ for Pd-103 and Au-198, and for Sm-153 $\alpha = 0.0068\ Gy^{-1}$.

	L-Pelletier <i>et al</i> (2017) (Pd-103)	Wang <i>et al</i> (2020) (Sm-153)	Katti <i>et al</i> (2018) (Au-198)
k (d^{-1})	0.55	0.63	0.38
m (d^{-1})	26.70	31.20	84.00
λ (d^{-1})	4.08E-02	4.37E-01	5.00E-02
S -value ($GyBq^{-1}\cdot d^{-1}$)	4.78E-12	7.58E-10	1.29E-09
ID_0	0.8	0.8	0.8
t_c (d)	7.00	6.02	9.2
$D(t_c)$ ($Gy\ h^{-1}$)	2.88E-02	2.66	3.53E-02
$SE_{min}(t_c)$	0.21	0.65	0.21

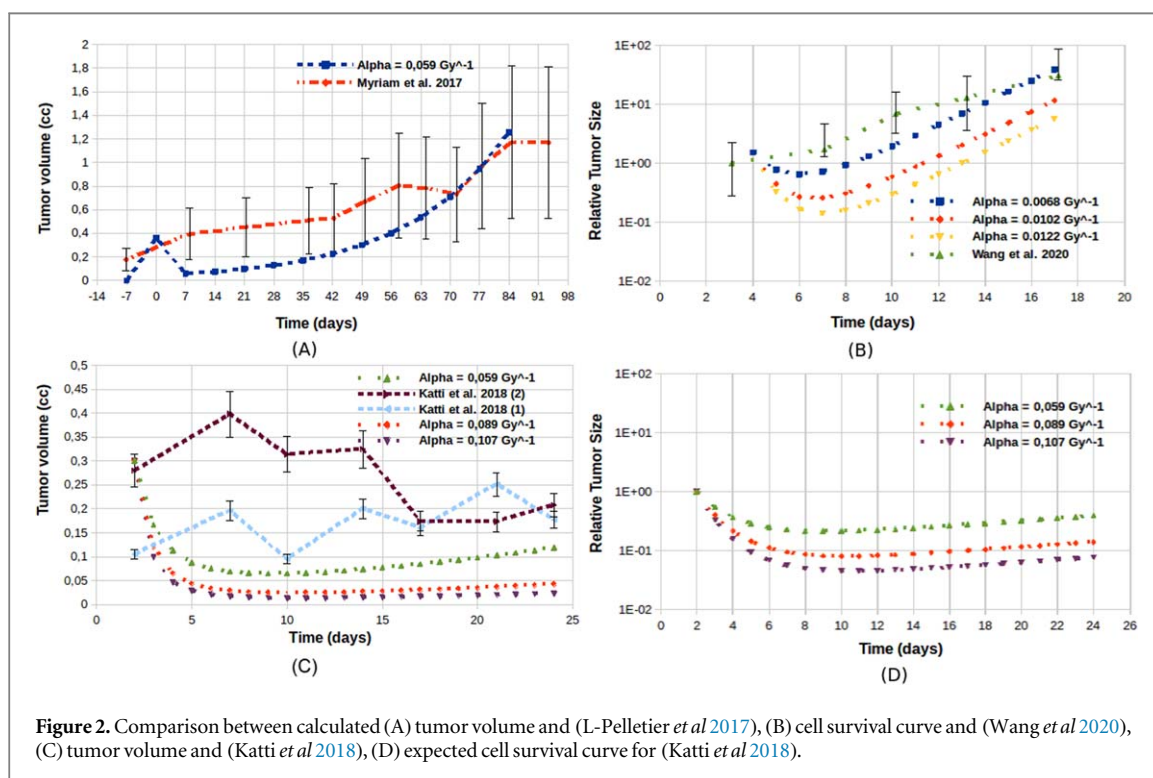


Figure 2. Comparison between calculated (A) tumor volume and (L-Pelletier *et al* 2017), (B) cell survival curve and (Wang *et al* 2020), (C) tumor volume and (Katti *et al* 2018), (D) expected cell survival curve for (Katti *et al* 2018).

relation: $D = S \cdot A$, where D is the absorbed dose, S is S -value and A is activity. The cell survival curves for tumor volume of 0.3, 0.6 and 1.0 c.c. were calculated for PC-3 cells in similar fashion as mentioned in case 1. The results are presented in figure 4(A).

- (iii) Case 3: Variable tumor cell type: Here we considered difference in cell lines, B16F10 ($\alpha = 0.0068\ Gy^{-1}$) and PC-3 ($\alpha = 0.059\ Gy^{-1}$) cells. The tumor volume of 0.3 c.c. and administered radioactivity of 600 MBq was considered for Pd-103. Here also the activity of the radionuclides was selected such that it resulted in similar absorbed dose. Hence, the activity for Au-198 and Sm-153 was estimated in similar fashion to that of Case 2. The calculated cell survival curves are presented in figure 4(B).

2.4. MIRDcell dosimetry tool

In this study the S -values calculated using the MIRDcell, version MIRDcell V2.1, dosimetry tool (Vaziri *et al* 2014) were used as reference. MIRDcell is a multidisciplinary tool provided by the MIRD committee of the Society of Nuclear Medicine and Molecular imaging. It can be used for bioeffect and microscale modeling purposes, such as calculation of S -values and surviving fraction, based on LQ formalism. Three type of radiation

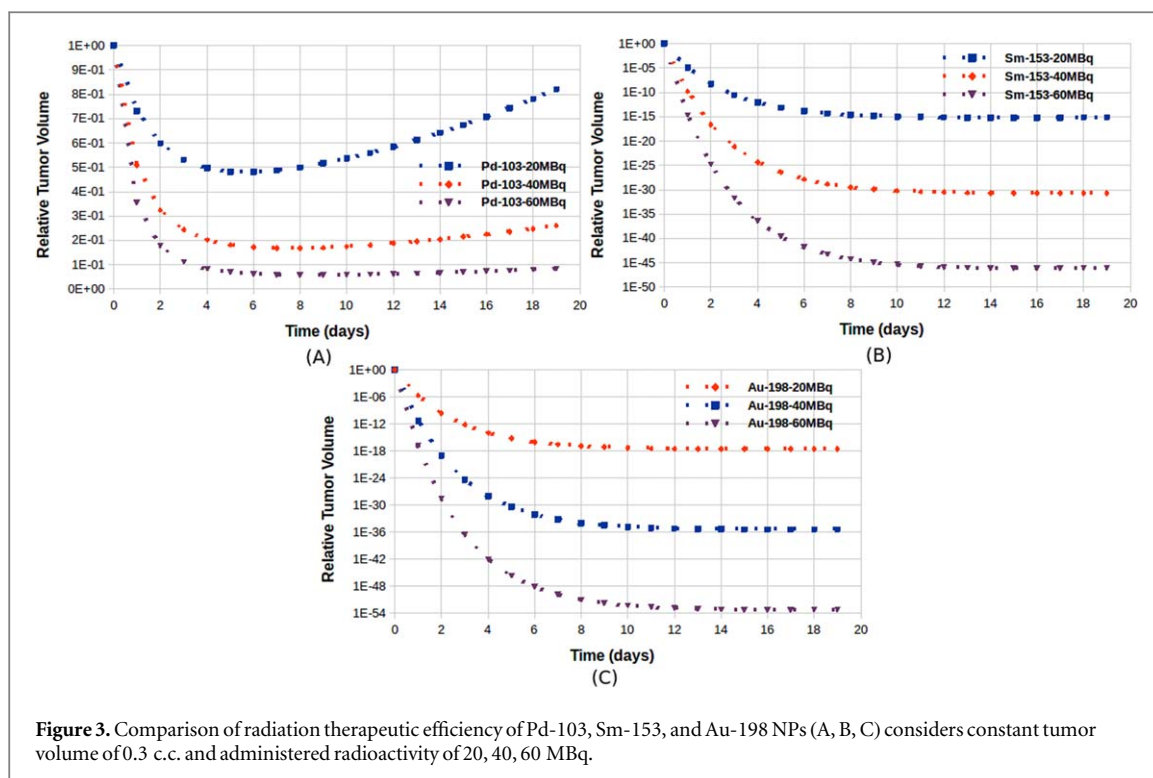


Figure 3. Comparison of radiation therapeutic efficiency of Pd-103, Sm-153, and Au-198 NPs (A, B, C) considers constant tumor volume of 0.3 c.c. and administered radioactivity of 20, 40, 60 MBq.

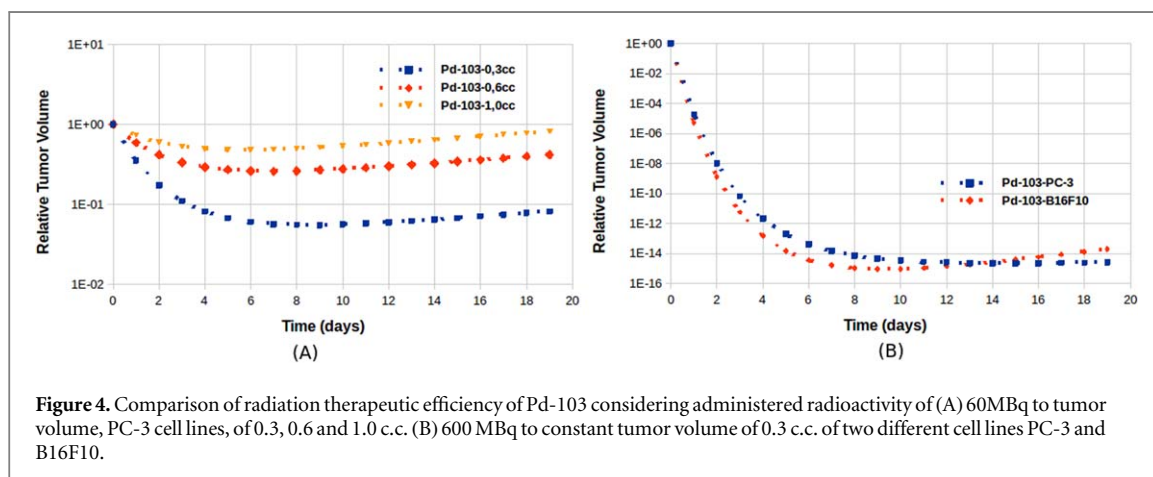


Figure 4. Comparison of radiation therapeutic efficiency of Pd-103 considering administered radioactivity of (A) 60MBq to tumor volume, PC-3 cell lines, of 0.3, 0.6 and 1.0 c.c. (B) 600 MBq to constant tumor volume of 0.3 c.c. of two different cell lines PC-3 and B16F10.

sources are supported by MIRDcell: (i) predefined MIRD radionuclides as source using full/average emission spectrum; (ii) monoenergetic particle emitter; or (iii) user defined radioactive source, and it only supports spherical volumes. We calculated cellular S -values by setting cell radius = 5 μm and nucleus radius = 4 μm . The calculations were performed for 5 source-target combinations as discussed in section 2.4. Whereas, the self dose for tumors ($S(T \leftarrow T)$) was estimated by setting cell radius = 0.42 cm (for 0.3 c.c.), 0.14 cm (for 0.6 c.c.) and 0.62 cm (for 1 c.c.) respectively and nucleus radius = 0. For both, cellular and tumor, S -value calculations full emission spectrum of predefined MIRD radionuclides: Pd-103, Sm-153 and Au-198 was used.

3. Results and discussion

3.1. Cellular S -values

The comparison between calculated cellular S -values and the S -values calculated from MIRDcell database (Vaziri *et al* 2014) is presented in table 2. Overall, the S -values calculated using EGSnrc were found in good agreement with MIRDcell database. In case of Pd-103 for all source-target combinations (($C \leftarrow C$), ($C \leftarrow CS$), ($N \leftarrow N$), ($N \leftarrow CY$) and ($N \leftarrow CS$)) the calculated S -values were found deviating by $\approx 14\%$ – 15% . For Sm-153 and Au-198 deviation less than 5% was observed for ($C \leftarrow C$), ($N \leftarrow N$), ($N \leftarrow CY$) and deviation $\approx 14\%$

was observed for (N ← CS) and (C ← CS). These variations can be due to: (i) differences in the emission spectrum used in calculation, and (ii) MIRDcell uses analytical methods for calculation of S-values. Whereas, EGSnrc performs detailed calculation by simulating the transport of electrons and photons. Seniwal *et al* (2020a), have reported a detailed study on discrepancies in S-value caused by differences in (i) Monte Carlo codes used in calculation, (ii) emission spectrum and also the similar deviation of S-values.

It can be observed that Sm-153 deposits the highest S-value within the source region ((C ← C) or (N ← N)) or in close proximity to it ((C ← CS) or (N ← CY)). Even for the target regions 1 μm far from the source region, (N ← CS), Sm-153 deposits higher absorbed dose per activity to the target region in comparison to Pd-103 and Au-198. It may be because Sm-153 emits Beta particles with mean and maximum energy of 223 and 807 keV, respectively (NNDC 2020). Seniwal *et al* (2020a), also reported this behavior for medium energy Beta particle emitters with the help of radial dose functions.

In comparison of S-values for Pd-103 and Au-198, it can be observed that for (C ← C), (N ← N) and (C ← CS) configurations Pd-103 deposits 2–3 times higher S-value than Au-198. This may be due to the Auger electrons and low energy x-rays, 35 keV (98%) (NNDC 2020, eckerman2008icrp), emitted by Pd-103. The Auger electrons deposit most of their energy within the source region or target region in close proximity to the source region. Whereas, Au-198 emits high energy Beta particles, 961 keV (98.99%) (NNDC 2020), which deposits most of the energy far from its origin. As most of the emitted particles escape the cell volume without depositing energy the S-value is almost equal for all source-target combinations. For (N ← CY) and (N ← CS) Pd-103 deposits less S-value in comparison to other configurations. It may be because the Auger electrons and the secondary electrons generated by low energy x-rays are absorbed within the source region or region near it before reaching the target volume. Seniwal *et al* (2020a) and Šefl *et al* (2015), have also reported similar behavior.

3.2. Surviving fraction and tumor volume

Table 3 presents the calculated washout rate (k), uptake rate (m) of NPs, tumor growth rate (λ), tumor S-value and fraction of injected dose retained in tumor volume (ID_0) from the experimental data available in L-Pelletier *et al* (2017), Katti *et al* (2018), Wang *et al* (2020). It also includes the critical time (t_c), critical dose rate ($D(t_c)$) and minimum survival fraction ($SF_{\min}(t_c)$) calculated using equation (6) and 7. The t_c , $D(t_c)$ and $SF_{\min}(t)$ were estimated by assuming $\alpha = 0.059 \text{ Gy}^{-1}$ for PC-3 cells and $\alpha = 0.0068 \text{ Gy}^{-1}$ for B16F10 cells, as these values of α provide best agreement between the calculated and experimental cell survival (or tumor volume) curves (see figure 2). From the table it can be observed that Mangiferin (MGF) functionalized Au-198 activated NPs have (a) lower washout rate, (b) higher uptake rate, and (c) equal ID_0 in comparison to cetuximab conjugated Sm-153 nanocapsules or PEG labeled Pd-103 NPs. The high value of λ and low value of α results in high $D(t_c)$ for B16F10-Luc cells in comparison to PC-3 cells. That is, high dose rate, greater than the one required for PC-3 cells, is required to balance between the sterilization and proliferation of B16F10-Luc. Also, melanoma B16F10-Luc cells are more aggressive, growth rate 10 times higher than PC-3 prostate cancer cells. From these observations it can be suggested that MGF is a better targeting agent and higher doses of radiation are required to eliminate B16F10 cells in comparison to PC-3 cells.

The calculated cell survival curves, using equation (1), and the tumor volume, using equation (5) are illustrated in figure 2, as well as the experimental data extracted from previously published work (L-Pelletier *et al* 2017, Katti *et al* 2018, Wang *et al* 2020). Globally all calculated and experimental curves show similar trend. However, some discrepancies are observed in early days of treatment. One hypothesis is that even if cell death starts to occur very early from the start of treatment, it must take some time for the tissue architecture to reorganize and a decrease in the volume of the tumor to be observed. This may be one of the causes of the delay in the tumor volume shrinkage observed in the experiments in relation to the calculated one. Reader must note that in these calculations NPs are treated as isotropic point sources uniformly and randomly sampled within the tumor volume. This may be a reasonable assumption for tumor volumes of size in cubic centimeters as the dimensions of nanoparticles are smaller by order of 10^{-7} in comparison to tumor size (diameter). Also the NPs with diameter in the range of 15–30 nm (with hydrodynamic diameter of 30–80 nm) can easily penetrate the vasculature of tumor and transport therapeutic payload to the tumor cells (Katti *et al* 2018). According to the findings of Laprise-Pelletier *et al* (2018b), after intratumoral injection within 24 h the NPs, carried in aqueous solution, diffuse slightly from the injection site within the extracellular matrix before getting internalized in the cell. However, it may not be a good assumption at cellular level, because the NPs accumulate within the cellular vesicles which are not uniformly distributed (Laprise-Pelletier *et al* 2018b). Also, it must be noted that in most of the pre-clinical studies available in literature Au is considered as biocompatible material to deliver radionuclides to the tumor cells, and do not investigate the dose enhancement or self absorption caused by Au. However, L-Pelletier *et al* (2017) used Pd-103 NPs coated with Au in order to exploit the enhancement in dose due to radiosensitization. In the calculations performed in this study we also do not consider the self absorption

(Cho *et al* 1999, Rivard *et al* 2017) or dose enhancement (Ngwa *et al* 2012, 2013, Martinov *et al* 2017, Sinha *et al* 2015) by material of NPs. However, the radionuclides: Pd-103, Sm-153 and Au-198 along with electrons emit photons of energy 20.6 keV (average) (Lechtman *et al* 2011), 103 keV (28%) (Jackson *et al* 2018) and 411 keV (93%) (Moreira *et al* 2010). These emitted photons/electrons on interaction with material of NPs, Au, can result in radiosensitization/self absorption. Consequently, it may result in increase/decrease in total absorbed dose within the tumor. The increase/decrease in tumor absorbed dose can lead to over-estimation/under-estimation of reduction in tumor volume.

Figure 2(A) illustrates the comparison between the calculated tumor volume and experimental data for Pd-103 NPs conjugated with PEG. The day -7 in figure 2(A) represents the day of measuring tumor volume before intratumoral injection (t_0) and day of injection (t_i) is day 0. The calculations consider PC-3 cell lines, $\alpha = 0.059, 0.089$ and 0.107 Gy^{-1} . The best agreement was observed for $\alpha = 0.059 \text{ Gy}^{-1}$, with $t_c = 7.0 \text{ d}$, and $\text{SF}_{\min} = 0.21$. The reduction in tumor volume is over-estimated for $\alpha = 0.089$ and 0.107 Gy^{-1} (results not shown). The Pd-103 NPs used by L-Pelletier *et al* (2017) had radioactive core of Pd-103 coated with gold (Au). Hence, the disagreement between the calculated and experimental curve might be consequence of not considering self-absorption or radiosensitization effect of Au. More detail on impact of size and concentration of AuNPs, and localization of NPs on radiosensitization for Pd-103 (brachytherapy seeds) can be found elsewhere (Lechtman *et al* 2011). Also, the mathematical model used in this study assumes, considering near complete repair of sublethal damage, a cell survival curve as an exponentially decreasing function of dose, which was useful in this work. However, a fully comprehensive model should include the quadratic mediated cell killing and Lea–Catcheside time factor (Lea and Catcheside 1942), G-factor, to account for DSB repair. Similarly, figure 2(B) illustrates the comparison between the calculated data and experimental data in terms of relative tumor volume (or surviving fraction). In figure 2(B) t_0 is day 3 and t_i is day 4. The calculations were performed for $\alpha = 0.0068, 0.0102$ and 0.0122 Gy^{-1} , B16F10 cell lines and the best agreement between the experimental and calculated results was for $\alpha = 0.0068 \text{ Gy}^{-1}$, with $t_c = 6.02 \text{ d}$, and $\text{SF}_{\min} = 0.65$. Figures 2(C), (D) reports the tumor volume and cell survival curves for Au-198 NPs, activated by neutron activation of Au, functionalized with MGF. In case of figures 2(C), (D) t_0 is day 2 and t_i is day 2. Also, figure 2(C) includes two set of experimental data, Katti *et al* 2018 (1) and Katti *et al* 2018 (2), published in Katti *et al* (2018). The calculations were performed for $\alpha = 0.059, 0.089$ and 0.107 Gy^{-1} , PC-3 cell lines. The best agreement between the experimental and calculated results was for $\alpha = 0.059 \text{ Gy}^{-1}$, with $t_c = 7.0 \text{ d}$, and $\text{SF}_{\min} = 0.21$. The discrepancies between calculated tumor volume curve and experimental data may be because we did not consider self-absorption or radiosensitization effect of Au. Other possible reasons for discrepancies between the calculated and experimental data are: (a) unavailability of detailed pharmacokinetic data, which effects the calculation of k and m (consequently the calculations), (b) large standard deviation in published experimental data, (c) discrepancies in emission spectrum used in calculations.

3.3. Comparison of radiotherapeutic efficiency of Pd-103, Sm-153 and Au-198 NPs

The comparison of S -values calculated using EGSnrc MC code and extracted from MIRDcell database (Vaziri *et al* 2014), for spherical tumors of volume 0.3, 0.6 and 1.0 c.c. using Pd-103, Sm-153 and Au-198 is illustrated in table 4. In these calculations tumor acted both as source and target ($T \leftarrow T$). The difference between the EGSnrc calculated S -values and MIRDcell database for Au-198 and Sm-153 was within 5%. However, for Pd-103 the difference up to 55%, with respect to MIRDcell, was observed. In order to investigate the cause of such high deviation we extracted the emission spectrum of Pd-103 from MIRDcell database and used it to estimate S -values using EGSnrc (not presented here). The calculated S -values, using emission spectrum from MIRDcell, were found equal to the S -values extracted from MIRDcell. Thus, the deviation observed between the MIRDcell database and EGSnrc calculated S -values, for Pd-103 (table 4), is caused by discrepancies in the emission spectrum. It was also found that MIRDcell makes use of the decay spectrum provided by ICRP-103 (Eckerman and Endo 2008). Similar variation in cellular S -values has been reported by Falzone *et al* (2017), while investigating the impact of input decay spectra on S -values.

From the calculated S -values it can be observed that Au-198 and Sm-153 deposit nearly equal absorbed dose per activity in all tumor volumes, whereas, according to table 2 Au-198 calculated S -values were lowest. This discrepancy is because at cellular level the high energy Beta particles emitted by Au-198 deposit most of their energy out of the cell. However, in this case all the emitted beta particles deposit their energy within the tumor volume. Pd-103 emissions are composed mainly of low energy monoenergetic photons and electrons and lack the relative high energy Beta emissions of Sm-153 and Au-198. Thus it can be explained why the Pd-103 deposits almost 10–100 times less S -value in comparison to Au-198 and Sm-153. So, it can be expected that higher radioactivity of Pd-103 is required to achieve radiotherapeutic effects similar to Au-198 and Sm-153.

Table 4. Comparison of calculated S-values ($\text{Gy Bq}^{-1} \cdot \text{s}^{-1}$) for different sizes of tumor using EGSnrc with respect to MIRDCell (Vaziri et al 2014).

	0.3 c.c.	0.6 c.c.	1.0 c.c.
S($T \leftarrow T$):	1.57E-	8.11E-	4.98E-
Au-198	10 (-5.37%)	11 (-4.70%)	11 (-4.40%)
MIRDCell	1.49E-10	7.75E-11	4.77E-11
S($T \leftarrow T$):	1.36E-	6.90E-	4.20E-
Sm-153	10 (-2.18%)	11 (-1.02%)	11 (-1.11%)
MIRDCell	1.33E-10	6.83E-11	4.15E-11
S($T \leftarrow T$):	4.36E-	2.30E-	1.46E-
Pd-103	12 (-39.24%)	12 (-47%)	12 (-55.5%)
MIRDCell	3.13E-12	1.56E-12	9.37E-13

Table 5. The critical time (t_c) (d), critical dose rate ($D(t_c)$) (Gy h^{-1}) and $\text{SE}_{\min}(t_c)$ calculated for variable tumor size (c.c.), type, administered activity (MBq) and radionuclide.

Case#	Radionuclide	Activity (MBq)	Tumor type	Volume (c.c.)	t_c (d)	$D(t_c)$ (Gy h^{-1})	$\text{SE}_{\min}(t_c)$	
1	Pd-103	20	PC3	0.30	8	3.53E-02	4.81E-01	
		40			9.5		1.67E-01	
		60			10.5		5.57E-02	
	Au-198	20	PC3	0.30	17	3.53E-02	3.00E-18	
		40			19		4.08E-36	
		60			20		5.35E-54	
	Sm-153	20	PC3	0.30	16.7	3.53E-02	6.66E-16	
		40			18.5		2.05E-31	
		60			19.5		6.06E-47	
	2	Pd-103	60	PC3	0.30	10.5	3.53E-02	5.51E-02
			60		0.60	8.9		2.59E-01
			60		1.00	7.7		4.77E-01
Au-198		0.17	PC3	0.30	10.5	3.53E-02	5.51E-02	
		0.17		0.60	8.9		2.59E-01	
		0.18		1.00	7.7		4.77E-01	
Sm-153		0.19	PC3	0.30	10.5	3.53E-02	5.51E-02	
		0.2		0.60	8.9		2.59E-01	
		0.21		1.00	7.7		4.77E-01	
3		Pd-103	600	PC-3	0.3	14.4	3.53E-02	2.28E-15
			600	B16F10	0.3	9.1		2.68E-01
		Au-198	16.7	PC-3	0.3	14.4	3.53E-02	2.28E-15
	16.7		B16F10	0.3	9.1	2.68E-01		8.93E-16
	Sm-153	19.2	PC-3	0.3	14.4	3.53E-02	2.28E-15	
		19.2	B16F10	0.3	9.1		2.68E-01	8.93E-16

The calculated critical time (t_c), critical dose rate ($D(t_c)$) and $\text{SE}_{\min}(t_c)$, using equation (6) and equation (7), for three cases considered to compare the radiotherapeutic efficiency of Pd-103, Sm-153 and Au-198 NPs (described in section 2.3) is presented in table 5.

Case 1: Variable radioactivity administered

From table 5 it can be observed that when tumor, 0.3 c.c., with PC-3 cell is treated with variable activity of 20, 40 and 60 MBq, for all radionuclides with increase in administered activity there is increase in t_c and decrease in $\text{SE}_{\min}(t_c)$. That is, the dose rate remains higher than $D(t_c)$ for a longer period of time when higher activities are administered. Since, $D(t_c)$ depends on tumor growth rate (λ) and radiosensitivity factor (α), it has a constant value of 3.53 cGy h^{-1} . The decrease in $\text{SE}_{\min}(t_c)$ is maximum for Au-198 (up to $5.35\text{E-}54$) and minimum for Pd-103 (up to $5.57\text{E-}02$). The value of t_c is almost equal for Au-198 and Sm-153 ($\approx 20 \text{ d}$ for 60 MBq), which is almost 7 times of their physical half life. Whereas, for Pd-103 the value of t_c is 10.5 d (for 60 MBq), which is less than one physical half life. It may be because of low dose rate of Pd-103 which cannot withstand the tumor proliferation rate for more than 10 d. Also, from the cell survival curves presented in figures 3(A)–(C), it can be observed that activity between 40–60 MBq of Pd-103 is required to treat 0.3 c.c. tumor. On the other hand, Sm-153 and Au-198, as medium and high energy Beta emitters, are capable of treating 0.3 c.c. tumors with activity as low as 20 MBq.

Case 2: Variable tumor volume

Here the therapeutic efficacy of Pd-103, Sm-153 and Au-198, variable administered activity and similar absorbed dose, was compared for variable tumor (PC-3 cell lines) sizes: 0.3, 0.6 and 1.0 c.c. The administered activity, keeping 60 MBq of Pd-103 as reference, for other radionuclides was selected such that they deposited equal dose, using the relation $\text{Dose} = S\text{-value} (T \leftarrow T) \times \text{Activity}$. It was found that ≈ 0.2 MBq of Au-198 and Sm-153 is required to deposit same dose as deposited by 60 MBq of Pd-103 (see table 5). Since, all radionuclides deposited similar absorbed dose, similar cell survival curves, t_c and $SE_{\min}(t_c)$ were obtained. The cell survival curves obtained using Pd-103 are presented in figure 4(A). It can be observed that 60 MBq of Pd-103 effectively treats 0.3 c.c. tumor ($t_c = 10.5$ d and $SE_{\min}(t_c) = 5.5E - 02$). Also, with increase in tumor volume, there is decrease in t_c (10.5 d to 7.7 d) and increase in $SE_{\min}(t_c)$ (0.055 to 0.5). Hence, it can be suggested that higher activities of Pd-103 are required to ablate 1.0 c.c. tumors, as tumor repopulation rate overtakes cell killing in 7.7 d (less than 1 half life), $t_c = 7.7$ d and $SE_{\min}(t_c) = 0.477$.

Case 3: Variable tumor cell type

figure 4(B) reports the cell survival curves for two different kind of tumors: (a) PC-3 prostate cancer cells, and (b) highly aggressive B16F10 melanotic melanoma cells, treated with 600 MBq of Pd-103. Here also the comparison of therapeutic efficiency was made considering that all radionuclide deposited equal absorbed dose and activity required for Au-198 and Sm-153 was estimated considering 600 MBq of Pd-103 as reference. It was found that 16.7 MBq, 19.2 MBq and 600 MBq of Au-198, Sm-153 and Pd-103 deposit equal absorbed dose to 0.3 c.c. tumor volume, and same absorbed dose resulted in similar cell survival curves. From table 5, it can be observed that with increase in radioresistance and growth rate of tumor cells there is an increase in $D(t_c)$ and $SE_{\min}(t_c)$ and decrease in t_c . Also, from figure 4(B) it can be appreciated that 600 MBq of Pd-103 almost completely ablate PC-3 tumor cells, $t_c = 14.4$ d and $SE_{\min}(t_c) = 2.28E - 15$. Whereas, in case of B16F10 melanoma cells the cell sterilization could not withstand cell repopulation rate after 9 d (t_c) with $SE_{\min}(t_c) = 8.93E - 16$.

In comparison it was found that (a) Au-198 has the highest dose rate (deposited highest dose per activity), (b) Au-198 and Sm-153 effectively reduce the cell surviving fraction of radioresistant tumors of size 0.3, 0.6 and 1.0 c.c. with low administered activity compared to Pd-103. Hence, it can be suggested that for large tumors Au-198 and Sm-153 are more effective than Pd-103.

4. Conclusion

The radioactive nanoparticles (NPs) have been reported as an alternative to low-dose-rate seed-based brachytherapy (BT). In this study we performed dosimetric calculations for NPs activated with Pd-103, Sm-153 and Au-198. The calculation was performed in three steps: (A) single cell dosimetry: the cellular S-values were calculated and compared with MIRDcell (Vaziri *et al* 2014) database; (B) cell survival (or tumor volume) curve calculations: the cell survival (or tumor volume) curves were calculated using equation (1) (or equation (5)) and compared with experimental data published in literature (L-Pelletier *et al* 2017, Katti *et al* 2018, Wang *et al* 2020); (C) The radiotherapeutic efficiency of these NPs were tested for variable (i) administered radioactivity, (ii) tumor volume, and (iii) tumor cell type.

At cellular level low energy x-ray emitter (Pd-103) and medium energy Beta-particle emitter (Sm-153) deposited maximum dose per activity within the cell. Whereas, the high energy Beta particles emitted from Au-198 leave the cell volume without depositing much energy. Also, the findings of this study support the mathematical model used to calculate the cell survival curves. It is able to reproduce the experimental results to a great extent. Better knowledge of uptake rate, washout rate of NPs, radiosensitivity and growth rate of tumors is important for these calculations. Also, self absorption of emitted radiation by NPs and dose enhancement caused by AuNPs must be considered in cell survival curve calculations.

Au-198 and Sm-153 effectively ablate large (≈ 1.0 c.c.), radio-resistant and aggressive tumors. However, considering the activity range studied here Pd-103 is only suitable for treatment of millimeter size tumors. Also, the use of MGF as targeting agent shows great potential over cetuximab and PEG due to its high uptake rate and low washout rate.

Acknowledgments

The following Brazilian institutions support this research project: Research Support Foundation of the State of Minas Gerais (FAPEMIG), Brazilian Council for Scientific and Technological Development (CNPq) and Coordination for the Capacitation of Graduated Personnel (CAPES). Professor T Fonseca is grateful for financial support provided by CNPq (processo no. 450 493/2019-9) and FAPEMIG (Projeto APQ-00083-18

Processo no. 2070.01.0002992/2018-30). Dr Lucas F Freitas and Professor A B Lugão would like to thank Fundação de Amparo à Pesquisa do Estado de São Paulo for the financial support (grant no. 2018/15598-2).

ORCID iDs

Baljeet Seniwal  <https://orcid.org/0000-0001-8250-5982>

Telma C F Fonseca  <https://orcid.org/0000-0003-2388-5174>

References

- Aranda-Lara L *et al* 2020 Radiolabeled liposomes and lipoproteins as lipidic nanoparticles for imaging and therapy *Chem. Phys. Lipids* **230** 104934
- Al-Yasiri A Y *et al* 2017 Mangiferin functionalized radioactive gold nanoparticles (MGF-198 AuNPs) in prostate tumor therapy: green nanotechnology for production, *in vivo* tumor retention and evaluation of therapeutic efficacy *Dalton Trans.* **46** 14561–71
- Brenner D J 2008 The linear-quadratic model is an appropriate methodology for determining isoeffective doses at large doses per fraction *Semin. Radiat. Oncol.* **18** 234–9
- Chanda N *et al* 2010 Radioactive gold nanoparticles in cancer therapy: therapeutic efficacy studies of GA-198AuNP nanoconstruct in prostate tumor-bearing mice *Nanomed.: Nanotechnol. Biol. Med.* **6** 201–9
- Cho S H *et al* 1999 Determination of the tissue attenuation factor along two major axes of a high dose rate (HDR) source *Med. Phys.* **26** 1492–7
- Dale R G *et al* 2007 *Radiobiological Modelling in Radiation Oncology* (London: British Institute of Radiology) pp 79–95
- Dale R and Alejandro C-F 2005 The radiobiology of conventional radiotherapy and its application to radionuclide therapy *Cancer Biother. Radiopharmaceuticals* **20** 47–51
- Dale R G 1985 The application of the linear-quadratic dose-effect equation to fractionated and protracted radiotherapy *Br. J. Radiol.* **58** 515–28
- Eckerman K and Endo AICRP 2008 ICRP Publication 107. Nuclear decay data for dosimetric calculations *Ann. ICRP* **38** 7–96
- Elqvist J *et al* 2016 Radiosensitivity of prostate cancer cell lines for irradiation from beta particle-emitting radionuclide ¹⁷⁷Lu compared to alpha particles and gamma rays *Anticancer Res.* **36** 103–9
- Falzone N *et al* 2017 Absorbed dose evaluation of Auger electron-emitting radionuclides: impact of input decay spectra on dose point kernels and S-values *Phys. Med. Biol.* **62** 2239
- Fonseca T C F *et al* 2020 MCMEG: Intercomparison exercise on prostate radiotherapy dose assessment *Radiat. Phys. Chem.* **167** 108295
- Gholami Y H *et al* 2020 A chelate-free nano-platform for incorporation of diagnostic and therapeutic isotopes *Int. J. Nanomed.* **15** 31–47
- Jackson M J *et al* 2018 International inter-comparison exercise on Sm-153 *J. Radioanal. Nucl. Chem.* **318** 107–15
- Katti K V *et al* 2018 Prostate tumor therapy advances in nuclear medicine: green nanotechnology toward the design of tumor specific radioactive gold nanoparticles *J. Radioanal. Nucl. Chem.* **318** 1737–47
- Kawrakow I 2000 Accurate condensed history Monte Carlo simulation of electron transport: I. EGSnrc, the new EGS4 version *Med. Phys.* **27** 485–98
- Laprise-Pelletier M *et al* 2017 Low-dose prostate cancer brachytherapy with radioactive palladium-gold nanoparticles *Adv. Healthcare Mater.* **6** 1601120
- Laprise-Pelletier M *et al* 2018a Gold nanoparticles in radiotherapy and recent progress in nanobrachytherapy *Adv. Healthcare Mater.* **7** 1701460
- Laprise-Pelletier M *et al* 2018b Intratumoral injection of low-energy photon-emitting gold nanoparticles: a microdosimetric Monte Carlo-based model *ACS Nano* **12** 2482–97
- Lea D E and Catcheside D G 1942 The mechanism of the induction by radiation of chromosome aberrations in *Tradescantia* *J. Genet.* **44** 216–45
- Lechtman E *et al* 2011 Implications on clinical scenario of gold nanoparticle radiosensitization in regards to photon energy, nanoparticle size, concentration and location *Phys. Med. Biol.* **56** 4631–47
- Leeuwen V *et al* 2018 The alfa and beta of tumours: a review of parameters of the linear-quadratic model, derived from clinical radiotherapy studies *Radiat. Oncol.* **13** 1–11
- Li W *et al* 2020 Intercomparison of dose enhancement ratio and secondary electron spectra for gold nanoparticles irradiated by x-rays calculated using multiple Monte Carlo simulation codes *Phys. Med.* **69** 147–63
- Martinov M P *et al* 2017 Heterogeneous multiscale Monte Carlo simulations for gold nanoparticle radiosensitization *Med. Phys.* **44** 644–53
- McMahon S J 2018 The linear quadratic model: usage, interpretation and challenges *Phys. Med. Biol.* **64** 01TR01
- Meyer T *et al* 2020 Peer-based credentialing for brachytherapy: application in permanent seed implant *Brachytherapy* **9** 794–6
- Moeendarbari S *et al* 2016 Theranostic nanoseeds for efficacious internal radiation therapy of unresectable solid tumors *Sci. Rep.* **6** 1–9
- Moreira D S *et al* 2010 Determination of ¹⁹⁸Au x-rays emission probabilities *Appl. Radiat Isotopes* **68** 1566–70
- Ngwa W *et al* 2012 Gold nanoparticle-aided brachytherapy with vascular dose painting: estimation of dose enhancement to the tumor endothelial cell nucleus *Med. Phys.* **39** 392–8
- Ngwa W *et al* 2013 *In vitro* radiosensitization by gold nanoparticles during continuous low-dose-rate gamma irradiation with I-125 brachytherapy seeds *Nanomed.: Nanotechnol. Biol. Med.* **9** 25–7
- NNDC 2020 National Nuclear Data Center (Accessed 12 October 2020) (<https://nndc.bnl.gov/ensdf/DatasetFetchServlet>)
- O'Donoghue J A 1994 The impact of tumor cell proliferation in radioimmunotherapy *Cancer* **73** 974–80
- Rivard M *et al* 2017 Supplement 2 for the 2004 update of the AAPM Task Group No. 43 Report: joint recommendations by the AAPM and GEC-ESTRO *Med. Phys.* **44** e297–338
- Schuemann J *et al* 2020 Roadmap for metal nanoparticles in radiation therapy: current status, translational challenges, and future directions *Phys. Med. Biol.* **65**
- Šefl M *et al* 2016 Impact of cell repopulation and radionuclide uptake phase on cell survival *Med. Phys.* **43** 2715–20
- Šefl M *et al* 2015 Calculation of cellular S-values using Geant4-DNA: the effect of cell geometry *Appl. Radiat. Isot.* **104** 113–23
- Seniwal B *et al* 2020 Comparison of dosimetric accuracy of acuros XB and analytical anisotropic algorithm against Monte Carlo technique *Biomed. Phys. Eng. Express* **6** 015035

- Seniwai B *et al* 2020a Microdosimetric calculations for radionuclides emitting β and α particles and Auger electrons *Appl. Radiat. Isot.* **166** 109302
- Seniwai B *et al* 2020b Monte Carlo assessment of low energy electron range in liquid water and dosimetry effects *Phys. Med.* **80** 363–72
- Shukla R *et al* 2012 Laminin receptor specific therapeutic gold nanoparticles (198AuNP-EGCg) show efficacy in treating prostate cancer *Proc. Natl Acad. Sci.* **109** 12426–31
- Sinha N *et al* 2015 Brachytherapy application with *in situ* dose painting administered by gold nanoparticle eluters *Int. J. Radiat. Oncol. Biol. Phys.* **91** 385–92
- Song G *et al* 2017 Emerging nanotechnology and advanced materials for cancer radiation therapy *Adv. Mater.* **29** 1700996
- Su W *et al* 2020 Radionuclide-labeled gold nanoparticles for nuclei-targeting internal radio-immunity therapy *Mater. Horiz.* **7** 1115–25
- Vaziri *et al* 2014 MIRD pamphlet No. 25: MIRDcell V2. 0 software tool for dosimetric analysis of biologic response of multicellular populations *J. Nucl. Med.* **55** 1557–64
- Wang J T W *et al* 2020 Neutron-irradiated antibody-functionalised carbon nanocapsules for targeted cancer radiotherapy *Carbon* **162** 410–22
- Wheldon T E *et al* 1991 The curability of tumours of differing size by targeted radiotherapy using ^{131}I or ^{90}Y *Radiother. Oncol.* **21** 91–9
- Wheldon T E and O'donoghue J A 1990 The radiobiology of targeted radiotherapy *Int. J. Radiat. Biol.* **58** 1–21